Aging of spermatogonial stem cells by Jnk-mediated glycolysis activation

Mito Kanatsu-Shinohara[a,b,1], Takuya Yamamoto[b,c], Hidehiro Toh[d], Yasuhiro Kazuki[e,f], Kanako Kazuki[e], Junichi Imoto[g,h], Kazuho Ikeo[g,h], Motohiko Oshima[i,j], Katsuhiko Shirahige[k], Atsushi Iwama[i,j], Yoichi Nabeshima[l], Hiroyuki Sasaki[d], and Takashi Shinohara[a,1]

[a]Department of Molecular Genetics, Graduate School of Medicine, Kyoto University, 606-8501 Kyoto, Japan; [b]Agency for Medical Research and Development–Core Research for Evolutional Science and Technology (AMED-CREST), Chiyodaku, 100-0004 Tokyo, Japan; [c]Department of Life Science Frontiers, Center for iPS Cell Research and Application, Kyoto University, 606-8507 Kyoto, Japan; [d]Division of Epigenomics and Development, Medical Institute of Bioregulation, Kyushu University, 812-8582 Fukuoka, Japan; [e]Chromosome Engineering Research Center, Tottori University, 683-8503 Yonago, Japan; [f]Department of Biomedical Science, Institute of Regenerative Medicine and Biofunction, Graduate School of Medical Science, Tottori University, 683-8503 Yonago, Japan; [g]Center for Information Biology, National Institute of Genetics, Mishima, 411-8540 Shizuoka, Japan; [h]Department of Genetics, SOKENDAI (The Graduate University for Advanced Studies), Mishima, 411-8540 Shizuoka, Japan; [i]Department of Cellular and Molecular Medicine, Graduate School of Medicine, Chiba University, 260-8670 Chiba, Japan; [j]Division of Stem Cell and Molecular Medicine, Center for Stem Cell Biology and Regenerative Medicine, Institute of Medical Science, University of Tokyo, 108-8639 Tokyo, Japan; [k]Laboratory of Genome Structure and Function, Institute for Quantitative Biosciences, The University of Tokyo, 113-0032 Tokyo, Japan; and [l]Laboratory of Molecular Life Science, Foundation for Biomedical Research and Innovation, 650-0047 Kobe, Japan

Edited by Ryuzo Yanagimachi, The Institute for Biogenesis Research University of Hawaii, Honolulu, HI, and approved July 3, 2019 (received for review March 25, 2019)

Because spermatogonial stem cells (SSCs) are immortal by serial transplantation, SSC aging in intact testes is considered to be caused by a deteriorated microenvironment. Here, we report a cell-intrinsic mode of SSC aging by glycolysis activation. Using cultured SSCs, we found that aged SSCs proliferated more actively than young SSCs and showed enhanced glycolytic activity. Moreover, they remained euploid and exhibited stable androgenetic imprinting patterns with robust SSC activity despite having shortened telomeres. Aged SSCs showed increased *Wnt7b* expression, which was associated with decreased Polycomb complex 2 activity. Our results suggest that aberrant *Wnt7b* expression activated c-*jun* N-terminal kinase (JNK), which down-regulated mitochondria numbers by suppressing *Ppargc1a*. Down-regulation of *Ppargc1a* probably decreased reactive oxygen species and enhanced glycolysis. Analyses of the *Klotho*-deficient aging mouse model and 2-y-old aged rats confirmed JNK hyperactivation and increased glycolysis. Therefore, not only microenvironment but also intrinsic activation of JNK-mediated glycolysis contributes to SSC aging.

aging | glycolysis | spermatogenesis

Because stem cells produce a large number of progenitors, they are often considered to be immortal. However, aged stem cells generally have impaired function, but the mechanism, particularly in terms of cell metabolism, is not well known. For example, although glycolysis promotes survival of hematopoietic stem cells (HSCs) in vitro (1), its impact on self-renewal division or aging has not been established. Metabolism in neural stem cells (NSCs) depends on glycolysis, but metabolic change during aging has not been determined (2). Unlike HSCs and NSCs, which are largely quiescent, spermatogonial stem cells (SSCs) continuously divide throughout the life span (3, 4), suggesting a distinct mode of aging.

SSC self-renewal depends on glycolysis (5). Despite the continuous self-renewal of SSCs, their number gradually declines during aging (6). However, SSC self-renewal continues long past the normal life span of the animal because SSCs proliferate for more than 3 y after being serially transplanted 9 times into immature testes (7). It was concluded that repeated transplantation into the young environment rejuvenated SSCs. Likewise, cultured SSCs, designated as germline stem (GS) cells, proliferated and produced offspring after 2 y of culture (10^{85}-fold expansion) (8, 9).

Although these results suggest that the fate of aging SSCs depends greatly on their microenvironment, cell intrinsic factors might also contribute to SSC aging because aging of many stem cell types is often accompanied by intrinsic cell changes. However, direct analysis of deteriorating SSCs in aged testes or serially transplanted testis cells is technically challenging due to their small number and lack of specific markers. To overcome these problems, we used 5-y-old GS cell cultures and analyzed their phenotypic changes. We reasoned that long-term GS cell cultures would mimic continuously dividing SSCs in vivo and hoped to uncover features specific to aged SSCs.

Results

Lack of Senescence and Defective Spermatogenesis of Aged GS Cells. Two GS cell lines with the *Egfp* transgene were cultured for 60 mo (60M-GS cells). Although we expected that telomere loss would occur at ∼34 mo after culture initiation (9), the cells

Significance

Spermatogenesis originates from spermatogonial stem cells (SSCs). Although aging testes lose SSCs, SSCs are considered immortal because they proliferate for 3 y by serial transplantation. However, analysis of aging is difficult because of their small number and lack of specific markers. Here, we used cultured SSCs as a model to study the aging process. We found that 5-y-old SSCs proliferated more actively with short telomeres. Despite maintaining SSC activity, they gradually lost sperm-forming potential. Hyperproliferation was associated with decreased Polycomb-repressive complex 2 activity, which activates the WNT7B-JNK pathway and alters SSC metabolism. These aged phenotypes were confirmed in mouse and rat aging models. Thus SSCs are virtually immortal but gradually lose sperm-forming potential, which is accompanied by abnormal proliferation, metabolism, and epigenetic alterations.

Author contributions: M.K.-S. and T.S. designed research; M.K.-S. and T.S. performed research; T.Y., H.T., Y.K., K.K., J.I., K.I., M.O., K.S., A.I., Y.N., and H.S. contributed new reagents/analytic tools; M.K.-S., T.Y., H.T., Y.K., K.K., J.I., K.I., M.O., K.S., A.I., H.S., and T.S. analyzed data; and M.K.-S. and T.S. wrote the paper.

The authors declare no conflict of interest.

This article is a PNAS Direct Submission.

Data deposition: The data reported in this paper have been deposited in the Gene Expression Omnibus (GEO) database, https://www.ncbi.nlm.nih.gov/geo [accession no. GSE120778 for Whole-Genome Bisulfite Sequencing (WGBS) and Chromatin Immunoprecipitation Sequencing (ChIP-seq) data] and in the DNA Data Bank of Japan, https://www.ddbj.nig.ac.jp/index-e.html (accession no. DRA007373 for RNA-seq data).

[1]To whom correspondence may be addressed. Email: mshioha@virus.kyoto-u.ac.jp or tshinoha@virus.kyoto-u.ac.jp.

This article contains supporting information online at www.pnas.org/lookup/suppl/doi:10.1073/pnas.1904980116/-/DCSupplemental.

Published online July 29, 2019.

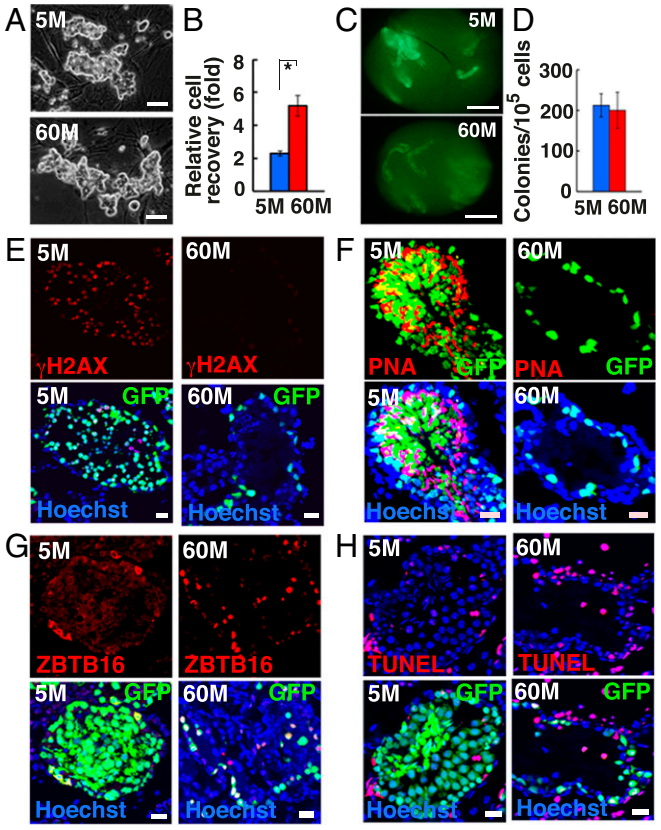

Fig. 1. Long-term culture of GS cells. (*A*) Appearance of 5M-GS and 60M-GS cells. (*B*) Cell recovery after 5 d ($n = 3$). (*C*) Appearances of W recipient testes. (*D*) Colony counts ($n = 8$–12). (*E*–*G*) Immuno- and lectin staining of recipient testes with anti-γH2AX (*E*), PNA (*F*), or ZBTB16 (*G*) antibodies. (*H*) TUNEL staining of recipient testes 3 mo after transplantation. (Scale bars: *A*, 50 μm; *C*, 1 mm; *E*–*H*, 20 μm.) Asterisk indicates statistical significance.

proliferated after this period without apparent changes (374–379 passages) (Fig. 1*A*). In contrast, 60M-GS cells proliferated more actively than 5M-GS cells (Fig. 1*B*), and responsiveness to GDNF or FGF2, both of which are SSC self-renewal factors, was enhanced (*SI Appendix*, Fig. S1*A*). Neither line was positive for the senescence-associated (SA) β-galactosidase stain (*SI Appendix*, Fig. S1*B*).

Flow cytometric analyses showed increased expression of ITGA6, but the remainder of the SSC markers did not change significantly (*SI Appendix*, Fig. S1*C*). RNA sequencing (RNA-seq) analyses showed that 60M-GS cells up-regulated several differentiation-associated genes, including *Kit*, while self-renewal–associated genes, such as *Bcl6b*, were more strongly expressed in 5M-GS cells (*SI Appendix*, Fig. S1*D* and Dataset S1). To test whether 60M-GS cells possessed SSC activity, cells were transplanted into infertile WBB6F1-W/W^{v} (W) mice (10). Analyses of the recipient testes revealed weaker fluorescence of 60M-GS cell transplants (Fig. 1*C*), and only a single layer of cells were found on the basement membrane (BM) (*SI Appendix*, Fig. S1*E*). Although SSC activity remained constant (Fig. 1*D* and *SI Appendix*, Table S1), no sperm developed when 30M-GS cells were transplanted (10^{105} to 10^{106}-fold expansion) (*SI Appendix*, Fig. S1 *E* and *F*). Interestingly, when we examined the recipient testes at 2 and 10 mo after transplantation, proliferation of CDH1^{+} spermatogonia from 30M-GS cells was significantly enhanced compared with that from 20M-GS cells (*SI Appendix*, Fig. S2). Because they were exposed to the same testis environment, this result also suggested that GS cells proliferate more actively in an autonomous manner.

Reverse transcription PCR (RT-PCR) analysis and immunostaining confirmed the lack of meiotic or haploid cells in testes with 60M-GS cells (Fig. 1 *E* and *F* and *SI Appendix*, Fig. S1 *G*–*I*). However, there were more ZBTB16^{+} spermatogonia in colonies of 60M-GS cell recipients (Fig. 1*G* and *SI Appendix*, Fig. S1*J*), and apoptosis was significantly enhanced (Fig. 1*H* and *SI Appendix*, Fig. S1*K*). Thus, GS cells maintained SSC activity, but could not produce sperm after 30 mo.

Telomere Shortening in GS Cells. Karyotype analysis revealed that ~64 to 68% of 5M-GS and 60M-GS cells contained 40 chromosomes (Fig. 2*A*). However, one of the lines showed a partial deletion of chromosome 17 (Fig. 2*B*). Because both lines had spermatogenic defects, it was unlikely that a partial deletion of chromosome 17 was responsible for the distinct phenotype of the 60M-GS cells. Next, WGBS was carried out (*SI Appendix*, Fig. S3*A*). The imprinting control regions showed no statistical differences in their DNA methylation levels (*SI Appendix*, Fig. S3*B*). The only exception was *Snrpn*, a maternally methylated gene, the methylation levels of which were significantly increased in the 60M-GS cells. However, real-time PCR showed no significant changes (*SI Appendix*, Fig. S3*C*). These results suggest that 60M-GS cells maintained androgenetic imprinting patterns.

However, a comparison in 500-kb windows revealed that genome-wide methylated CpG residue (mCpG) levels slightly increased in 60M-GS cells (74.5 vs. 75.7%). Because these values were somewhat higher than that of fresh KIT^{-} undifferentiated spermatogonia (73.9%) (11), DNA methylation appeared to increase during culture. When we compared the methylation levels in these cells strictly, 13,556 differentially methylated regions (DMRs) showed increased DNA methylation in 60M-GS cells, but 5M-GS cells contained only 858 DMRs that showed increased DNA methylation (Dataset S2). The increase in DNA methylation occurred in all chromosomes, but DMRs (5M > 60M) were predominantly found in introns, while DMRs (60M > 5M) were more frequently located in intergenic regions (*SI Appendix*, Fig. S3*D*). This difference depended on the GC content. While mCpG levels were similar (~60–75%) in GC-rich regions (GC content > 44%), increased methylation levels were found in GC-poor regions (GC content < 39%), which often corresponded to the constitutive nuclear lamina-associated domains (cLADs) (*SI Appendix*, Fig. S3*E*). cLADs help to organize

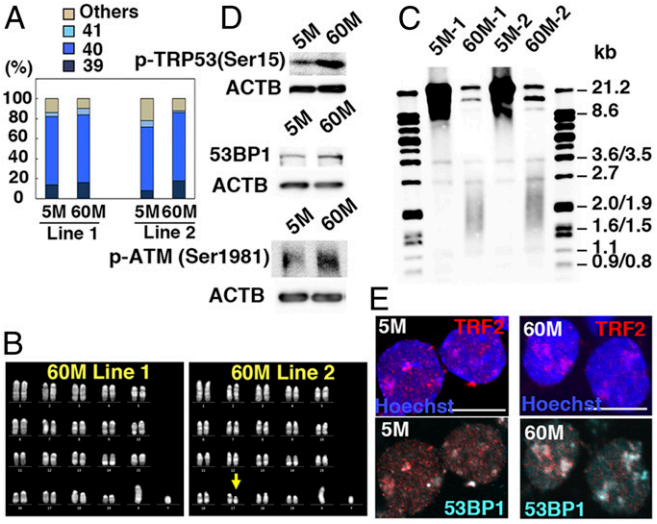

Fig. 2. Telomere shortening in GS cells. (*A*) Karyotypic analyses ($n = 50$). (*B*) Quinacrine mustard and Hoechst 33258 staining of 60M-GS cells. (*C*) Telomere length assay. (*D*) Western blot analyses of p-TRP53(Ser15) (*Top*), 53BP1 (*Middle*), and p-ATM (*Bottom*). (*E*) Immunostaining of GS cells showing colocalization of 53BP1 and TRF2. (Scale bar: *E*, 10 μm.)

chromosomes inside the nucleus, are associated with gene repression (12), and contain fewer genes compared with GC-rich regions. Because similar methylation patterns around cLADs have been found in fresh spermatogonia (11), 60M-GS cells appear to maintain basic nuclear architecture.

We examined telomere length because late generation (~G6) telomerase knockout (KO) mice have defective spermatogenesis (13). Telomeres were significantly shorter in 60M-GS cells (Fig. 2*C*). Because their lengths did not change between 54 and 60 mo, 60M-GS cells were thawed to confirm that the telomere length did not change even at 72 mo (*SI Appendix*, Fig. S4*A*), suggesting that GS cells proliferate for 18 mo even with very short telomeres. To examine telomerase expression level, we carried out real-time PCR analysis and found that 60M-GS cells express significantly lower levels of *Tert* and *Terc*, both of which are important components of telomerase (*SI Appendix*, Fig. S4*B*).

Because chromosomal abnormalities cause DNA damage, we performed Western blotting analyses and found that markers of DNA damage (53BP1, phosphorylated TRP53, and ATM) are more strongly expressed in 60M-GS cells (Fig. 2*D*). This was likely due to telomere damage because TRF2 (a telomere marker) and 53BP1 signals often colocalized (Fig. 2*E*). Therefore, 60M-GS cells proliferated despite DNA damages.

Increased c-Jun N-Terminal Kinase (JNK) Activity Promotes GS Cell Proliferation. To understand the mechanism of enhanced proliferation of 60M-GS cells, we performed Western blotting and examined the activation levels of major signaling pathways and cell cycle regulators. The expression levels of p-JNK1-3 (MAPK8-10), p-MAPK14, and nonphosphorylated CTNNB1, an activated form of CTNNB1, were enhanced in 60M-GS cells (Fig. 3*A*). Regarding cell cycle-related molecules, 60M-GS cells up-regulated CDKN2A (p19ARF) (Fig. 3*A*), although its high expression did not interfere with spermatogonia proliferation (14).

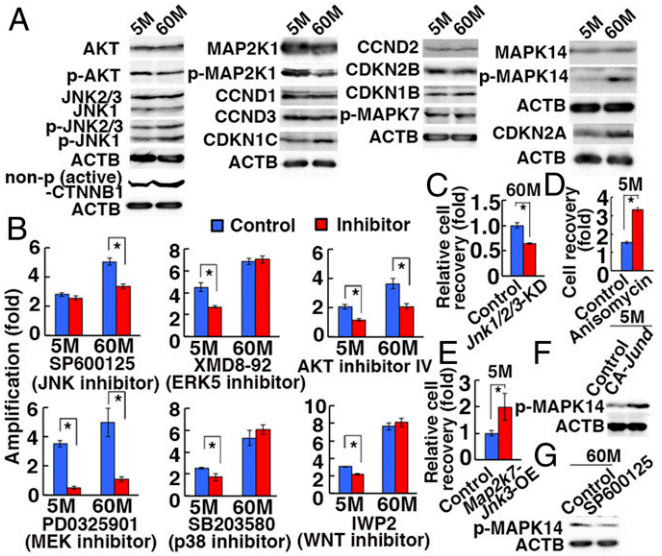

Fig. 3. Enhanced JNK signaling in 60M-GS cells. (*A*) Western blot analyses. (*B*) Cell recovery after treatment with indicated inhibitors for 4 d ($n = 3$). (*C*) Reduction of 60M-GS cell recovery 4 d after cotransduction with shRNA against *Jnk1*, *Jnk2*, and *Jnk3* ($n = 3$). (*D*) Enhanced proliferation of 5M-GS cells 2 d after anisomycin treatment ($n = 3$). (*E*) Enhanced proliferation of 5M-GS cells 4 d after *Map2k7-Jnk3* OE ($n = 3$). (*F*) Western blot analyses of 5M-GS cells 15 h after transfection of CA *Jund*. (*G*) Western blot analyses of 60M-GS cells 6 h after SP6000125 treatment. Asterisks indicate statistical difference.

Chemical inhibitor studies revealed that SP600125 abrogated the proliferation of 60M-GS cells without influencing 5M-GS cells (Fig. 3*B*). By contrast, SB203580 and XMD8-92 inhibited the growth of 5M-GS cells, but not 60M-GS cells, suggesting that 5M-GS cells depended more on the p38 mitogen-activated protein kinase (MAPK) and MAPK7 (ERK5) pathways. Because these results suggest the involvement of the JNK pathway in enhanced proliferation of 60M-GS cells, we confirmed this by triple depletion of *Jnk1/2/3* by short hairpin RNA (shRNA) in 60M-GS cells, which significantly decreased cell recovery (Fig. 3*C* and *SI Appendix*, Fig. S5*A*). Moreover, anisomycin, an activator of the JNK and p38 MAPK pathways, enhanced proliferation of 5M-GS cells (Fig. 3*D*). We also transfected *Map2k7-Jnk3* into 5M-GS cells to activate the JNK pathway. Recovery of cells after transfection was significantly enhanced after *Map2k7-Jnk3* overexpression (OE) (Fig. 3*E*). When we specifically expressed constitutively active (CA) *Jund*, which is the most strongly expressed *Jun* family gene in GS cells, the cells showed increased MAPK14 phosphorylation (Fig. 3*F*). Because MAPK14 phosphorylation was inhibited by SP600125 (Fig. 3*G*), JNK activation was necessary and sufficed for MAPK14 phosphorylation. However, MAPK14 activation per se did not appear to be responsible for hyperproliferation because SB203580 inhibited the proliferation of 5M-GS, but not 60M-GS cells (Fig. 3*B*). These results raised a possibility that JNK activation is responsible for enhanced proliferation of 60M-GS cells.

Decreased Polycomb Repressive Complex 2 (PRC2) Activity and Increased WNT7B in 60M-GS Cells. Because the culture environment remained the same during the entire period, the enhancement of JNK signaling was likely caused by an autonomous cell mechanism. Although RNA-seq data did not show apparent genes involved in JNK signaling, Chromatin Immunoprecipitation Sequencing (ChIP-seq) using H3K4me3 and H3K27me3 antibodies showed that H3K27me3 peaks were significantly decreased in the promoter regions of *Wnt7b* and *Wnt9b* (Fig. 4*A*). While *Wnt9b* expression was not detectable in either type of GS cells by RT-PCR, real-time PCR analyses showed that *Wnt7b* was significantly up-regulated in 60M-GS cells (Fig. 4*B*). The enrichment of H3K27me3 in the promoter region of *Wnt7b* was confirmed by ChIP analysis (Fig. 4*C*). Although we noted similar H3K27me3 enrichment in the *Tert* and *Terc* promoters, H3K4me3 enrichment was also found in the *Tert* promoter, which suggested that telomerase is regulated in a different manner from *Wnt7b* (*SI Appendix*, Fig. S4*C*).

Hence, we investigated the involvement of *Wnt7b* in GS cell proliferation by *Wnt7b* OE. Cell recovery was significantly enhanced by *Wnt7b* OE (Fig. 4*D*). By contrast, *Wnt7b* knockdown (KD) reduced 60M-GS cell proliferation (Fig. 4*E* and *SI Appendix*, Fig. S5*B*). Because *Wnt7b* activates both canonical and noncanonical WNT signaling, we transfected *Wnt7b* in 5M-GS cells and found that *Wnt7b* OE induced JNK phosphorylation (Fig. 4*F* and *SI Appendix*, Fig. S6*A*). Likewise, *Wnt7b* KD in 60M-GS cells reduced JNK phosphorylation (Fig. 4*G* and *SI Appendix*, Fig. S6*B*). Therefore, *Wnt7b* expression level was closely associated with JNK phosphorylation in GS cells.

Genome-wide analyses of ChIP sequence data revealed ~10-fold more H3K4me3 peaks than H3K27me3 peaks in both 5M-GS and 60M-GS cells. The number of H3K27me3 peaks was slightly decreased in 60M-GS cells (*SI Appendix*, Fig. S7*A*). Although previous studies using fresh spermatogonia showed bivalent loci with underlying DNA hypomethylation (15, 16), genomic regions with decreased DNA methylation levels in 5M-GS and 60M-GS cells had high H3K4me3 levels regardless of H3K27me3 levels (*SI Appendix*, Fig. S7*B*).

Interestingly, the widths and heights of the H3K4me3 and H3K27me3 peaks changed in an opposite manner: H3K4me3 peaks became wider and higher in 60M-GS cells, and the ratio

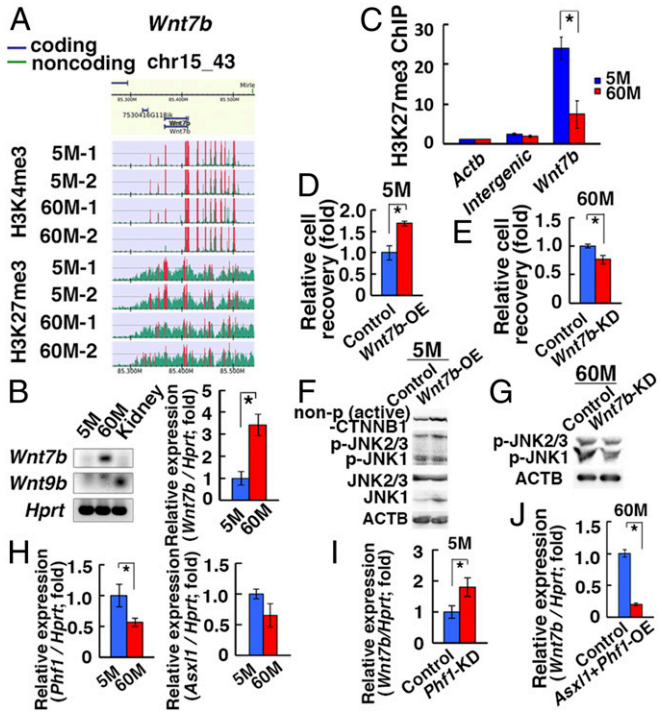

Fig. 4. Induction of *Wnt7b* after long-term culture. (*A*) ChIP-Seq analyses of the *Wnt7b* promoter region. The green histogram indicates the ChIP-read line, and the region above the threshold is highlighted in red. The red regions in ChIP-read line indicate peak regions. (*B*) RT- and real-time PCR analyses of *Wnt7b* and *Wnt9b* (n = 5–9). (*C*) ChIP analyses of the *Wnt7b* promoter region. (*D*) Enhanced cell recovery of 5M-GS cells 7 d after *Wnt7b* OE (n = 3). (*E*) Reduced cell recovery of 60M-GS cells 7 d after *Wnt7b* KD (n = 3). (*F*) Western blot analyses of 5M-GS cells 7 d after *Wnt7b* OE. (*G*) Western blot analyses of 60M-GS cells 4 d after *Wnt7b* KD. (*H*) Real-time PCR analyses of *Phf1* and *Asxl1* (n = 8, for *Phf1*; n = 4, for *Asxl1*). (*I*) Real-time PCR analyses of *Wnt7b* 3 d after *Phf1* KD in 5M-GS cells (n = 8). (*J*) Real-time PCR analyses of *Wnt7b* 3 d after cotransfection of *Phf1* and *Asxl1* in 60M-GS cells (n = 8). Asterisks indicate statistical difference.

of height to width decreased (average 95.4%). By contrast, H3K27me3 peaks became narrower and lower in 60M-GS cells, and the ratio of height to width increased (average 106.2%) (*SI Appendix*, Fig. S7*C*). Consequently, while there were more genes associated with H3K4me3 in 5M-GS cells, 60M-GS cells had relatively fewer genes associated with H3K27me3. This change in histone modification pattern resulted in a smaller number of genes with bivalent modification in 60M-GS cells than in 5M-GS cells (1,216 vs. 958) (Dataset S3). Gene Ontology (GO) analyses indicated that genes enriched in H3K27me3 only and bivalent promoters were commonly involved in positive regulation of the metabolic process, animal organ development, and the cellular metabolic process (*SI Appendix*, Fig. S7*D*). We hypothesized that the globally decreased activity of the PRC2 complex was responsible for the aging of SSCs.

The PRC2 complex consists of several components, including EZH1/2 and SUZ12 (17). We examined the expression of PRC2 components using real-time PCR and found that *Phf1* was significantly decreased in 60M-GS cells (Fig. 4*H*). Therefore, we focused on *Phf1*. PHF1 modulates the enzymatic activity of PRC2 or recruits PRC2 to specific genomic loci (17). To test the impact of *Phf1*, we depleted *Phf1* in 5M-GS cells and noted a significant increase in *Wnt7b* expression (Fig. 4*I* and *SI Appendix*, Fig. S5*C*). However, *Phf1* OE alone in 60M-GS cells did not change *Wnt7b* expression significantly. Because *Asxl1*, another PRC2 component, was down-regulated in 60M-GS cells (Fig. 4*H*), we cotransfected *Phf1* and *Asxl1*, which resulted in significant reduction of *Wnt7b* expression (Fig. 4*J*). Therefore, a decrease in PRC2 activity may partly contribute to the increased *Wnt7b* expression in 60M-GS cells.

Reduced Reactive Oxygen Species (ROS) and Mitochondria Dysfunction in 60M-GS Cells. Because ROS accumulate in many aged cells (18), ROS levels were measured in GS cells. Contrary to our expectations, ROS levels were significantly lower in 60M-GS cells than in 5M-GS cells (n = 3) (*SI Appendix*, Fig. S8*A*), as were H_2O_2 levels (n = 3) (*SI Appendix*, Fig. S8*B*). To study this mechanism, several ROS inhibitors were used. We found that mitochondrial respiratory chain inhibitors, such as antimycin C and rotenone, and the NAD(P)H oxidase (NOX) inhibitors diphenyleneiodonium (DPI) and apocynin, significantly suppressed proliferation of both cell types (*SI Appendix*, Fig. S8*C*).

Although *Nox1* deficiency impairs SSC self-renewal (19), *Nox1* significantly increased in 60M-GS cells (*SI Appendix*, Fig. S8*D*). Next we analyzed the status of the mitochondria, which are another major source of ROS. As expected, Mitotracker staining showed a significant reduction of mitochondria in 60M-GS cells (*SI Appendix*, Fig. S8 *E* and *F*). This decrease was also suggested by decreased mitochondrial DNA (0.6-fold) (*SI Appendix*, Fig. S8*G*). Therefore, the reduction in mitochondrial activity is likely responsible for the decreased ROS formation in 60M-GS cells.

60M-GS Cells Have Reduced Mitochondrial Function. Because 60M-GS cells showed significant loss of mitochondria and GO analyses suggested metabolic changes, we reasoned that 60M-GS cells had altered metabolic activity. As expected, maximal respiration and spare capacity were significantly reduced in 60M-GS cells (*SI Appendix*, Fig. S9*A*). An increased glycolytic pathway appeared to compensate for this defect because 2-deoxy-D-glucose (2DG), a glucose analog that inhibits glycolysis, suppressed 60M-GS cell proliferation more significantly, suggesting that 60M-GS cells depended more heavily on glycolysis than 5M-GS cells (*SI Appendix*, Fig. S9*B*). Indeed, glycolysis and glycolytic capacity were significantly increased in 60M-GS cells (*SI Appendix*, Fig. S9*C*). As expected, *Map2k7-Jnk3* OE increased the extracellular acidification rate (ECAR) in 5M-GS cells (*SI Appendix*, Fig. S9*D*).

To examine the mechanism underlying mitochondrial defects, we searched for the genes responsible for this phenomenon by real-time PCR. Through screening of genes involved in mitochondria-related genes, we found that *Ppargc1a* was significantly down-regulated in 60M-GS cells (*SI Appendix*, Fig. S9*E*). Western blot analyses confirmed this result (*SI Appendix*, Fig. S9*F*). Because *Ppargc1a* positively regulates the number and activity of mitochondria (20), decreased *Ppargc1a* expression is likely responsible for mitochondrial deficiency. Indeed, while *Ppargc1a* KD significantly reduced mitochondria in 5M-GS cells (*SI Appendix*, Figs. S5*D* and S9*G*), *Ppargc1a* OE increased their number in 60M-GS cells (*SI Appendix*, Fig. S9*H*). *Ppargc1a* expression levels were also closely related with ROS levels; *Ppargc1a* KD decreased ROS (*SI Appendix*, Fig. S9*I*), while *Ppargc1a* OE increased ROS (*SI Appendix*, Fig. S9*J*).

To examine whether enhanced JNK signaling was involved in ROS regulation and mitochondria activity, we transfected CA *Jund* in 5M-GS cells and found that the transfected cells decreased *Ppargc1a* expression (*SI Appendix*, Fig. S9*K*). In contrast, when SP600125 was added to inhibit JNK in 60M-GS cells, *Ppargc1a* significantly increased (*SI Appendix*, Fig. S9*L*). Consistent with these observations, anisomycin decreased mitochondrial staining and ROS generation in 5M-GS cells (*SI Appendix*, Fig. S9 *M* and *N*), suggesting that JNK was necessary and sufficient for *Ppargc1a* expression. These results provided evidence that down-regulation of mitochondrial activity in 60M-GS cells was caused by JNK activation.

JNK Hyperactivation and Enhanced Glycolysis in Spermatogonia of Rodent Aging Models. To confirm the in vitro findings, we analyzed rodent aging models. *Klotho* KO mice show many features of aged mice, including infertility (21). *Klotho* KO testis was significantly smaller by 7 wk after birth (*SI Appendix*, Fig. S10*A*). These testes contained significantly fewer tubules with PNA^+ haploid cells (*SI Appendix*, Fig. S10 *B* and *C*). However, immunostaining indicated increased proliferation of $ZBTB16^+$ cells (*SI Appendix*, Fig. S10*D*). Although the number of mitotic KIT^+ cells was comparable (*SI Appendix*, Fig. S10*E*), 53BP1 expression was significantly elevated in *Klotho* KO mice (*SI Appendix*, Fig. S10*F*), suggesting more DNA damage. Germ cell apoptosis was elevated in spermatocytes without apparent changes in Sertoli cells (*SI Appendix*, Fig. S10 *G–K*).

We also analyzed Brown Norway (BN) rats, the best representative rodent model of human testicular aging (22). In this model, the frequency of atrophied testes increases with age; 5 of 10 animals had bilateral atrophied testes when testes were collected from 24-mo-old animals (*SI Appendix*, Fig. S11*A*). The atrophied testes showed significantly lower weights than those from young (8 wk) or aged animals (*SI Appendix*, Fig. S11*B*). Histological analysis showed very few germ cells (*SI Appendix*, Fig. S11*C*). However, they still contained a small number of mitotic $ZBTB16^+$ spermatogonia that proliferate more actively than those in young testes (*SI Appendix*, Fig. S11*D*).

Because of the 60M-GS cell phenotype, the expression of molecules involved in GS cell aging was evaluated. Although *Phf1* and *Wnt7b* expression did not show statistical significance in *Klotho* KO mice, we noted decreased PHF1 expression and increased WNT7B expression in BN rats (Fig. 5 *A* and *B*). Consistent with the increased glycolysis in aged GS cells, HK1 expression increased in undifferentiated spermatogonia of both models (Fig. 5*C* and *SI Appendix*, Fig. S11*D*). Because HK1 mediates an irreversible step of glycolysis, this result suggested that aged spermatogonia depend more heavily on glycolysis. Indeed, spermatogonia from *Klotho* KO testes showed enhanced glycolytic capacity (Fig. 5*D*). Moreover, lactate production was increased in BN rat spermatogonia from atrophied testes (Fig. 5*E*). Because maximal respiratory capacity did not change significantly in newborn *Klotho* KO mice (*SI Appendix*, Fig. S10*L*), we carried out flow cytometric analyses and found that *Klotho* KO germ cells had significantly less mitochondrial staining (*SI Appendix*, Fig. S10*M*), suggesting that *Klotho* KO mitochondria at this stage can still accommodate metabolic changes before they exhibit defective spermatogenesis.

To evaluate the SSC activity in a functional manner, we performed spermatogonial transplantation. Cell recovery from *Klotho* KO testes significantly decreased (*SI Appendix*, Fig. S10*N*). Analysis of recipients revealed significant enrichment of SSCs in *Klotho* KO testes (Fig. 5 *F* and *G*). Because it is possible that SSC enrichment was caused by a loss of differentiating germ cells, we performed serial transplantation to confirm the enhanced self-renewal activity of *Klotho* KO SSCs. Assuming 10% colonization efficiency (23), the multiplication of colony numbers (total regenerated colony number × 10/primary colony number) significantly increased (Fig. 5*G*). Consistent with increased proliferation, *Klotho* KO spermatogonia showed increased expression of phosphorylated JNK (Fig. 5*H* and *SI Appendix*, Fig. S6*C*). We also confirmed increased JNK phosphorylation in $GFRA1^+$ spermatogonia in 2-y-old atrophied BN testes (*SI Appendix*, Fig. S11*D*). Thus, JNK hyperactivation and increased glycolysis appear to be the common features of aged rodent SSCs.

Discussion

An interesting feature of 60M-GS cells was the lack of apparent senescence. Both lines proliferated even with very short telomeres but maintained SSC activity. However, both lines gradually lost sperm-forming potential. Although we currently do not know whether lack of senescence and loss of spermatogenic potential are related to each other, at least 2 possibilities exist to explain the loss of sperm-forming potential. First, it is possible that failure to complete spermatogenesis was caused by telomere shortening because spermatogenic arrest was also found in late generation (~G6) telomerase KO mice the spermatogenesis of which was interrupted at the onset of meiosis (13). DNA damages found around the telomeres in 60M-GS cells may similarly inhibit meiosis. However, indirect influences on spermatogenesis in the KO mice cannot be excluded completely, and transplantation of telomerase KO mice into normal recipients is necessary to define the impact of telomerase in meiosis. The second possibility is the increased *Wnt7b* expression. Because Wnt family genes promote proliferation of spermatogonia (24), increased *Wnt7b* may have promoted self-renewal and inhibited meiosis. Thus, SSCs are virtually immortal but the mechanism underlying the loss of haploid cell-forming capacity needs to be determined in future.

Another notable feature of aged GS cells was their enhanced proliferation. Our analysis suggested that reduced PRC2 activity caused by *Phf1* down-regulation is responsible for *Wnt7b* up-regulation and JNK hyperactivation. Although age-induced changes in H3K27 methylation levels have previously been reported for HSCs and muscle stem cells (25), the peaks become broader and more intense upon aging. By contrast, H3K27me3 peaks become narrower and lower in 60M-GS cells. Although we noted *Phf1* down-regulation in 60M-GS cells, the reason for this difference from other stem cell types and why *Phf1* and *Asxl1* were down-regulated remain to be determined. Because PHF1 and ASXL1/BAP1 are involved in DNA repair (26, 27), increased DNA damage during aging may influence their expression levels. In the germline, PRC2 is important for regulating SSC number (28). Our results now suggest that PRC2 may play additional roles during aging.

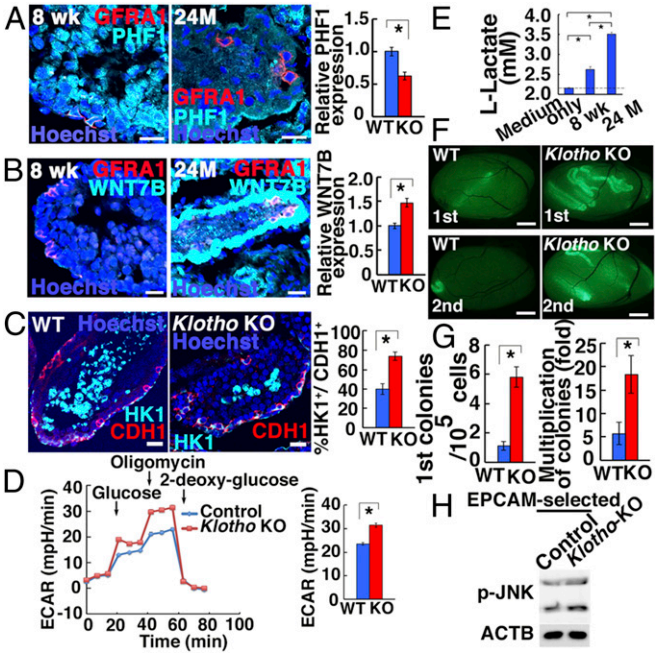

Fig. 5. Functional analyses of SSCs in *Klotho* KO mice and BN rats. (*A* and *B*) Immunostaining of BN rat testes by GFRA1 and PHF1 (*A*: $n = 22$) or WNT7B (*B*: $n = 20$–21). (*C*) Immunostaining of *Klotho* KO mouse testes by HK1 and CDH1 ($n = 25$ to 29). (*D*) ECAR of *Klotho* KO spermatogonia ($n = 21$ to 22). (*E*) Lactate production of BN rat spermatogonia ($n = 6$). (*F*) Appearance of primary (*Top*) and secondary (*Bottom*) recipient testes. (*G*) Colony counts ($n = 16$, for first recipients; $n = 12$, for second recipients). (*H*) Western blot analyses of phosphorylated JNK in EPCAM-selected *Klotho* KO testis cells ($n = 7$). (Scale bars: *A–C*, 20 μm; *F*, 1 mm.) Asterisks indicate statistical difference.

Activation of the WNT-JNK pathway caused abnormal metabolism in GS cells. Although AKT activation promotes glycolysis in GS cells (5), we found that JNK activation enhances glycolysis in 60M-GS cells. On the other hand, 60M-GS cells had lower levels of ROS. We initially thought that decreased NOX1 activity was responsible for this change because NOX1 is important for SSCs (19). However, *Nox1* was expressed more strongly in 60M-GS cells. In addition, ROS reduction was caused by augmentation of WNT-JNK signaling via mitochondrial defect. When this signaling pathway was activated in 5M-GS cells, the number of mitochondria decreased significantly. Down-regulation of *Ppargc1a* was ultimately responsible for the decrease in mitochondria activity. Considering that 60M-GS cells proliferate more actively despite the down-regulation of mitochondria-derived ROS, NOX-derived ROS probably play more important roles in SSC self-renewal. How the difference in the origin of ROS influences GS cell proliferation is a next important question.

Undifferentiated spermatogonia in *Klotho* KO mice and aged BN rats also show JNK phosphorylation and enhanced glycolysis. Although we could not carry out transplantation experiments with BN rats due to lack of donor cell markers, serial transplantation of *Klotho* KO testes showed more frequent self-renewing divisions. Moreover, the increased generation of secondary colonies of *Klotho* KO SSCs also suggests that the aging phenotype was not rescued by transplantation into the wild-type environment (primary recipients). These defects are probably caused by intrinsic defects in the germ cells because only germ cells express KLOTHO (29). On the other hand, while down-regulation of PHF1 and increased WNT7B expression in BN rats were confirmed, *Wnt7b* did not change significantly in *Klotho* KO mice. We speculate that *Klotho* mutations might have occurred downstream of *Wnt7b* signaling.

Our study suggests that cell-autonomous factors also contribute to SSC aging. Although we cannot completely exclude the possible involvement of other factors, we think that down-regulation of PRC2 activity likely contributed to the aged phenotype of 60M-GS cells by activating WNT7B-JNK signaling. One of the next important unsolved questions is how the telomeres are maintained in aged SSCs. Since there were no apparent karyotype abnormalities, SSCs must have a unique machinery to protect telomere fusions. Because the *Klotho* KO mouse phenotype is caused by hyperphosphatemia caused by abnormal calcium metabolism (21), further investigation of the link between calcium metabolism and glycolysis may also reveal the mechanisms of SSC aging. Studies of these issues are warranted in the future, which opens up new possibilities for controlling germ cell aging and infertility.

Materials and Methods

Cell Culture. GS cells were derived from C57BL/6 Tg14(act-EGFP)OsbY01 on a DBA/2 background (green) (M. Okabe, Osaka University, Osaka, Japan) (8). GS cell culture conditions were previously described (8). The cells were maintained on mouse embryonic fibroblasts treated with mitomycin C (Sigma). SA β-galactosidase activity was examined as described previously (30).

To determine the effects of chemicals, GS cells were treated with allopurinol (50 μM; Sigma), antimycin A (5 μM; Santa Cruz), rotenone (1 μM; Sigma), DPI (1 μM; Sigma), apocynin (1 mM; TCI), L-NAME (100 μM; Santa Cruz), anisomycin (300 ng/mL Santa Cruz), H_2O_2 (30 μM; Wako). Dimethyl sulfoxide (Sigma) or medium was used as a control. For analyses of the signal transduction pathway, GS cells were treated with SP600125 (13.3 μM; Selleck), XMD8-92 (1.67 μM; Tocris), AKT inhibitor IV (26.7 μM; Calbiochem), PD0325901 (1 μM; Stemgent), SB203580 (10 μM; Selleck), or IWP2 (0.5 μM; Stemgent). In some experiments, 2DG (5 mM; Wako) was used to study the impact of glycolysis.

Statistical Analyses. Results are presented as means ± SEMs. Significant differences between means for single comparisons were determined using the Student's *t* test. Multiple comparison analyses were performed using ANOVA followed by Tukey's HSD test.

Accession Numbers. All of the sequencing data generated in this study have been deposited in the GEO and DDBJ databases (GSE120778 for WGBS and ChIP-seq and DRA007373 for RNA-seq data, respectively).

ACKNOWLEDGMENTS. We thank Ms. S. Ikeda, M. Kataba, and S. Sakurai for technical assistance. Financial support was provided by the Ministry of Education, Culture, Sports, Science, and Technology, Japan (18H05281, 19H05750, and 17H05639). This research is also supported by the Platform Project for Supporting in Drug Discovery and Life Science Research (Platform for Drug Discovery, Informatics, and Structural Life Science) from the Japan Agency for Medical Research and AMED-CREST (JP18gm1110008).

1. K. Ito, T. Suda, Metabolic requirements for the maintenance of self-renewing stem cells. *Nat. Rev. Mol. Cell Biol.* **15**, 243–256 (2014).
2. E. A. Stoll *et al*., Aging neural progenitor cells have decreased mitochondrial content and lower oxidative metabolism. *J. Biol. Chem.* **286**, 38592–38601 (2011).
3. D. G. de Rooij, L. D. Russell, All you wanted to know about spermatogonia but were afraid to ask. *J. Androl.* **21**, 776–798 (2000).
4. M. L. Meistrich, M. E. A. B. van Beek, "Spermatogonial stem cells" in *Cell and Molecular Biology of the Testis*, C. C. Desjardins, L. L. Ewing, Eds. (Oxford University Press, 1993), pp. 266–295.
5. M. Kanatsu-Shinohara *et al*., Myc/Mycn-mediated glycolysis enhances mouse spermatogonial stem cell self-renewal. *Genes Dev.* **30**, 2637–2648 (2016).
6. X. Zhang, K. T. Ebata, B. Robaire, M. C. Nagano, Aging of male germ line stem cells in mice. *Biol. Reprod.* **74**, 119–124 (2006).
7. B. Y. Ryu, K. E. Orwig, J. M. Oatley, M. R. Avarbock, R. L. Brinster, Effects of aging and niche microenvironment on spermatogonial stem cell self-renewal. *Stem Cells* **24**, 1505–1511 (2006).
8. M. Kanatsu-Shinohara *et al*., Long-term proliferation in culture and germline transmission of mouse male germline stem cells. *Biol. Reprod.* **69**, 612–616 (2003).
9. M. Kanatsu-Shinohara, T. Shinohara, Spermatogonial stem cell self-renewal and development. *Annu. Rev. Cell Dev. Biol.* **29**, 163–187 (2013).
10. R. L. Brinster, J. W. Zimmermann, Spermatogenesis following male germ-cell transplantation. *Proc. Natl. Acad. Sci. U.S.A.* **91**, 11298–11302 (1994).
11. N. Kubo *et al*., DNA methylation and gene expression dynamics during spermatogonial stem cell differentiation in the early postnatal mouse testis. *BMC Genomics* **16**, 624 (2015).
12. B. van Steensel, A. S. Belmont, Lamina-associated domains: Links with chromosome architecture, heterochromatin, and gene repression. *Cell* **169**, 780–791 (2017).
13. M. T. Hemann *et al*., Telomere dysfunction triggers developmentally regulated germ cell apoptosis. *Mol. Biol. Cell* **12**, 2023–2030 (2001).
14. M. L. Churchman, I. Roig, M. Jasin, S. Keeney, C. J. Sherr, Expression of arf tumor suppressor in spermatogonia facilitates meiotic progression in male germ cells. *PLoS Genet.* **7**, e1002157 (2011).
15. S. S. Hammoud *et al*., Chromatin and transcription transitions of mammalian adult germline stem cells and spermatogenesis. *Cell Stem Cell* **15**, 239–253 (2014).
16. S. S. Hammoud *et al*., Transcription and imprinting dynamics in developing postnatal male germline stem cells. *Genes Dev.* **29**, 2312–2324 (2015).
17. R. Margueron, D. Reinberg, The Polycomb complex PRC2 and its mark in life. *Nature* **469**, 343–349 (2011).
18. T. Finkel, The metabolic regulation of aging. *Nat. Med.* **21**, 1416–1423 (2015).
19. H. Morimoto *et al*., ROS are required for mouse spermatogonial stem cell self-renewal. *Cell Stem Cell* **12**, 774–786 (2013).
20. S. Austin, J. St-Pierre, PGC1α and mitochondrial metabolism: Emerging concepts and relevance in ageing and neurodegenerative disorders. *J. Cell Sci.* **125**, 4963–4971 (2012).
21. Y. Nabeshima, Discovery of alpha-Klotho unveiled new insights into calcium and phosphate homeostasis. *Proc. Jpn. Acad. Ser. B Phys. Biol. Sci.* **85**, 125–141 (2009).
22. C. Wang, A. Leung, A. P. Sinha-Hikim, Reproductive aging in the male brown-Norway rat: A model for the human. *Endocrinology* **133**, 2773–2781 (1993).
23. M. Nagano, M. R. Avarbock, R. L. Brinster, Pattern and kinetics of mouse donor spermatogonial stem cell colonization in recipient testes. *Biol. Reprod.* **60**, 1429–1436 (1999).
24. A. P. G. Lombardi *et al*., Physiopathological aspects of the Wnt/β-catenin signaling pathway in the male reproductive system. *Spermatogenesis* **3**, e23181 (2013).
25. I. Beerman, D. J. Rossi, Epigenetic control of stem cell potential during homeostasis, aging, and disease. *Cell Stem Cell* **16**, 613–625 (2015).
26. Z. Hong *et al*., A polycomb group protein, PHF1, is involved in the response to DNA double-strand breaks in human cell. *Nucleic Acids Res.* **36**, 2939–2947 (2008).
27. O. Abdel-Wahab *et al*., Deletion of Asxl1 results in myelodysplasia and severe developmental defects in vivo. *J. Exp. Med.* **210**, 2641–2659 (2013).
28. W. Mu, J. Starmer, A. M. Fedoriw, D. Yee, T. Magnuson, Repression of the soma-specific transcriptome by Polycomb-repressive complex 2 promotes male germ cell development. *Genes Dev.* **28**, 2056–2069 (2014).
29. S. A. Li *et al*., Immunohistochemical localization of Klotho protein in brain, kidney, and reproductive organs of mice. *Cell Struct. Funct.* **29**, 91–99 (2004).
30. F. Debacq-Chainiaux, J. D. Erusalimsky, J. Campisi, O. Toussaint, Protocols to detect senescence-associated beta-galactosidase (SA-betagal) activity, a biomarker of senescent cells in culture and in vivo. *Nat. Protoc.* **4**, 1798–1806 (2009).